RSC Advances

ROYAL SOCIETY OF CHEMISTRY

www.rsc.org/advances

Journal Name

ARTICLE

A simple strategy to modify the porous structure of plasma electrolytic oxidation coatings on magnesium

Received 00th January 20xx,
Accepted 00th January 20xx

DOI: 10.1039/x0xx00000x

www.rsc.org/

T.S.N. Sankara Narayanan and Min Ho Lee*

A simple strategy to modify the porous structure of the oxide coating formed on Mg by plasma electrolytic oxidation (PEO) is addressed. Post-treatment of PEO coated Mg using 3 M NaOH at 60 °C for 1 h modifies its porous structure, helps to seal the smaller pores and decrease the size of medium and bigger size pores, increases the surface roughness but provides a better homogeneity of the surface, changes its chemical nature, improves its corrosion resistance in Hank's balanced salt solution, facilitate apatite growth in simulated body fluid and promotes cell viability and growth in cell culture media.

Introduction

Plasma electrolytic oxidation (PEO) is a proven approach to impart desirable surface characteristics on Mg and its alloys that are warranted for biomedical applications.[1, 2] The PEO coating strongly integrates with the substrate and serves as an excellent base to improve adhesion of bioactive coatings subsequently deposited over them. The formation of micropores and cracks in the oxide layer are inevitable during PEO. Permeation of corrosive medium through them to the base metal limits the extent of corrosion protection offered by the PEO coatings. In a recent review, the various strategies adopted to improve the corrosion resistance of PEO coatings on Mg and its alloys are addressed.[3] Deposition of another layer either by sol-gel coating[4-9] or by the deposition of a biodegradable polymer coating[10-12] could completely cover the porous structure of PEO coatings. Nevertheless, the cracks in the sol-gel coating or the fine pores in the polymer coating could still allow infiltration of the corrosive medium through them and attack the base metal. Deposition of coatings with a higher thickness seems appropriate; but cohesive failure and, cracks in the coating due to the build-up of stress are the major concerns.[13] Moreover, they might affect the bioactivity of the PEO coated Mg/Mg alloys. Hence, it is imperative that the strategy adopted should help to effectively seal the pores of the PEO coating without impairing the bioactivity. Alkaline treatment is widely used to modify the surface of Ti and Mg alloys to impart bioactivity and to promote apatite formation.[14-18] For Ti and its alloys, an alkaline treatment in 5 M NaOH for 24 h followed by heat-treatment at 600 to 800 °C for 1 to 5 h enables the formation of sodium titanate with a porous network.[14, 15] When exposed to simulated body fluid (SBF), ion exchange between Na^+ ions released from sodium titanate and H_3O^+ ions present in the SBF leads to the formation of hydrated titania with Ti-OH groups while an increase in pH facilitates an increase in ionic product activity, both of which favours nucleation of apatite. Based on thermodynamic and kinetic considerations, formation of apatite and its rate of deposition from SBF is promoted by an increase in pH.[19] Since Mg and its alloys are highly active, it is generally believed that there is no need to form a $Mg(OH)_2$ layer by adopting a separate treatment.[16] It is well known that deposition of PEO coatings could considerably reduce the dissolution of Mg in SBF when compared to its uncoated counterpart.[1-3] As a result, the extent and rate of increase in pH as well as the apatite formation is decreased, warranting methods to improve the bioactivity of PEO coated Mg and its alloys. Anawati et al.[18] have reported that an alkaline post-treatment using 0.25 M NaOH at 80 °C for 90 min has induced the formation of a nano-size platelet shaped $Mg(OH)_2$ layer, which increased the effective surface area and facilitated the precipitation of uniform apatite layer. An improvement in apatite forming ability has also been observed on pure Mg following the formation of a $Mg(OH)_2$ layer when treated using pure H_2O at 100 °C for 15 min.[16] However, an increase in treatment time from 15 to 30 min has lead to the formation of more cracks and defects in the $Mg(OH)_2$ layer, which negatively influenced the corrosion resistance.[16] Li et al.[20] have employed an alkaline post-treatment using 1 to 3 M NaOH followed by surface silanization to effectively seal the pores of PEO coating deposited on Mg. However, the chemical nature of the modified surface formed after alkaline post-treatment is not completely understood. Moreover, the ability of the modified layer using high concentrations of NaOH to promote apatite formation has not been studied earlier. The present

Department of Dental Biomaterials and Institute of Biodegradable Materials, Institute of Oral Bioscience and School of Dentistry (plus BK21 program), Chonbuk National University, Jeonju 561-756 South Korea
* Corresponding author. Tel/Fax: +82 0632704040;
E-mail: lmh@chnbuk.ac.kr (M.H. Lee);
tsnsn@rediffmail.com (T.S.N. Sankara Narayanan)

paper aims to explore alkaline post-treatment to modify the porous structure of PEO coating on Mg, in terms of its characteristics and corrosion behaviour in Hank's balanced salt solution (HBSS). Moreover, the study also aims to evaluate the ability of the modified surface to promote apatite deposition from SBF as well as its cytocompatibility when compared to the PEO coated and uncoated Mg.

Materials and methods

Commercially pure Mg ingot (99.93% purity) (Sincere East Foreign Trade Corp., China) was sliced into small blocks and subsequently cut to small pieces of dimension 20 mm x 15 mm x 3 mm. To remove the surface oxide layer and other contaminants, they were mechanically polished using SiC coated abrasive (grit size: 600) paper, cleaned using ethanol for 10 min in an ultrasonic cleaner and dried. An alkaline silicate solution prepared using 5 g/l NaOH and 15 g/l Na_2SiO_3 was used as the electrolyte. PEO was performed under direct current mode at 250 V for 2 min using Pt as the cathode. During PEO, the temperature of the electrolyte was controlled at < 40 °C using a water bath. After deposition, the coated Mg samples were rinsed thoroughly using deionized water and dried. The PEO coated Mg samples were subjected to an alkaline post-treatment using 3 M NaOH at 60 °C for 1 h. After post-treatment, they were rinsed thoroughly with hot deionized water to remove the alkali residues and dried. The surface morphology of the PEO coated Mg before and after alkaline post-treatment was assessed using a field emission scanning electron microscope (FE-SEM) (Hitachi - Analytical UHR Schottky Emission Scanning Electron Microscope, Model: SU-70). Their chemical composition was determined by energy dispersive X-ray analysis (EDAX). Quantitative estimation of pore density of the PEO coated Mg before and after post-treatment was made using a standard image processing technique. The corresponding FE-SEM images with an image area of 71.516 mm^2 were used for the analysis. The pore pixels were identified by their characteristics after subtracting them from the background. The pore density was estimated based on the number of pixels in the pore area and expressed in terms of number of pixels/mm^2. Thin film X-ray diffraction (TF-XRD) measurement (PANalytical X'pert MRD) was used to identify the various phases present in these coatings. The TF-XRD patterns were recorded using Cu K_α radiation at a glancing angle of 1°. The surface topography of PEO coated Mg and those modified by alkaline post-treatment was assessed using atomic force microscopy (AFM) (Bruker NanoScope V multimode 8 scanning probe microscopy) in tapping mode. The 3-dimensional AFM images were acquired over a scanning area of 5 x 5 μm. Fourier-transform infrared (FT-IR) (Perkin Elmer® Spectrum™ GX systems) spectra of these samples were recorded in the spectral range of 4000-400 cm^{-1} to ascertain the nature of functional groups present in these samples.

Potentiodynamic polarization study was employed to determine the corrosion behaviour of PEO coated Mg and those subjected to alkaline post-treatment, in HBSS at 27 °C. Uncoated Mg was used as a control to compare the extent of corrosion protection offered by them. The potentials were referenced to Ag/AgCl/saturated KCl electrode. To evaluate the long-term corrosion behavior, uncoated Mg, PEO coated Mg and those subjected to alkaline post-treatment were immersed in HBSS at 37 °C for 168 h. The change in pH of the HBSS was monitored to compare their rate of corrosion. The extent of corrosion attack after removal of the corrosion products using 200 g/l CrO_3 modified with the addition of 10 g/l $AgNO_3$ was assessed by SEM. The details of polarization study and immersion corrosion test were elaborated in our earlier papers.[12, 21] The apatite forming ability of uncoated Mg, PEO coated Mg and those post-treated using 3 M NaOH was evaluated by immersing them in SBF at 37 °C for 240 h. EDAX analysis was performed at various regions of these samples to identify the type of elements present. In addition, FT-IR spectra were recorded to assess the chemical nature of the compounds formed after immersion in SBF.

MC3T3-E1 cells, a mouse calvaria-derived osteoblast-like cell line, obtained from American Type Culture Collection (ATCC, Manassas, VA, USA) were used to evaluate the cytocompatibility of uncoated Mg, PEO coated Mg and those post-treated using 3 M NaOH at 60 °C for 1 h. Minimum Essential Medium Eagle (α-MEM) (Sigma, USA) supplemented with 10% fetal bovine serum (FBS) (Gibco Co., USA) and 1% antibiotic was used as the cell culture medium. Since Mg is highly active in cell culture medium, the cytocompatibility was evaluated by an indirect assay method as per ISO 10993-5 standard. To prepare the extracts, the uncoated and PEO coated Mg samples were incubated in cell culture medium with a surface area of the sample to the extraction medium ratio of 1.25 cm^2/ml for 72 h under physiological conditions (37 °C; 5 % CO_2; 95% relative humidity) as per ISO 10993-12 standard. After treatment for 72 h, the samples were removed from the cell culture medium, washed with deionized water and dried. The surface morphology and chemical composition of the surface layer were assessed using FE-SEM and EDAX analysis, respectively while the chemical nature of their surface was ascertained by FT-IR spectroscopy. The extracts were centrifuged at 14,000 rpm for 15 min and supernatant solution was considered as 100% extract. This extract is further diluted with α-MEM to prepare 10% and 25% extracts. MC3T3-E1 cells were seeded in 24-well plates with a cell density of 1 x 10^4 cells/ml of the medium and incubated for 24 h under physiological conditions to ensure proper cell adhesion. The medium was subsequently replaced with 100 μl of 10% and 25% extracts as well as with 1 ml of negative control (cell culture medium alone) and the MC3T3-E1 cell lines were incubated again under physiological conditions for 1, 2 and 3 days. At the end of each time interval, 10 μL of 2-(2-methoxy-4-nitrophenyl)-3-(4-nitrophenyl)-5-(2,4-disulfophenyl)-2H-tetrazolium monosodium salt (WST-8) solution was added into each well and again incubated for 2 h. The absorbance of each well was

measured at 490 nm using an enzyme-linked immunosorbent assay (ELISA) microplate reader. Calculation of the relative growth rate (RGR) of the cells was made using the following equation:

$$RGR\ (\%) = (OD_t / OD_n) \times 100\%$$

Where OD_t refers to the optical density of the samples of the present study and OD_n corresponds to the optical density of the negative control. The cell morphology and extent of cell growth after the stipulated period of cell culture followed by crystal violet staining were assessed using an inverted phase contrast microscope.

Results and discussion

The surface morphology of the PEO coating deposited on Mg using the alkaline silicate electrolyte at 250 V for 2 min reveals a porous structure (Figs. 1(a)), which is one of the most common attributes of such type of coatings. The mechanism of PEO of Mg alloys is explained elsewhere.[1,22] The naturally formed oxide layer on Mg is not dense (Pilling-Bedworth ratio of 0.81). When the potential is applied, during the initial stages of PEO (first 30 s), the naturally formed oxide film thickens with the evolution of tiny oxygen bubbles, representing the anodizing stage. With a further increase in time (from 30 s to 80 s), small sparks starts to appear all over the surface, which is accompanied by an increase in the extent of oxygen evolution, suggesting the breakdown of the oxide layer by the microscopic plasma discharges. The life-time of these sparks is very low. Beyond this time interval (from 80 s to 100 s), the number of sparks are decreased except for the occurrence of a few large sparks at selective locations. The final stage of the coating process (from 100 s to 120 s) is evidenced by the disappearance of sparks and oxygen evolution. The high temperature and pressure generated locally at the plasma discharge sites modify the oxide layer. The growth of the PEO coating involves several stages that include melting and reflow of the oxide layer assisted by the plasma discharges, diffusion of ions present in the electrolyte to the growth front, re-solidification, sintering and densification due to continuous melting and cooling of the oxide layer respectively caused by the plasma discharges and the electrolyte. The ejection of the molten oxide and its rapid cooling by the electrolyte generates the porous structure with volcano like features.[22] The pore density and diameter is largely a function of electrolyte composition, electrical parameters and treatment time used for deposition. In the present study, the pore diameter of the PEO coating varies from 0.10 to 1.20 μm (Fig. 1(b)). EDAX analysis indicates the presence of O (38.86 at. %), Mg (46.99 at. %) and Si (14.15 at. %) as the major elements (Table 1), possibly due to the formation of $Mg(OH)_2$, MgO, Mg_2SiO_4 and $MgSiO_3$. During PEO, anodic dissolution of magnesium generates Mg^{2+} ions (equation 1). They react with the OH^- ions formed at the interface to produce $Mg(OH)_2$ (equation 2). The conversion of $Mg(OH)_2$ to MgO is favoured by the high temperature and high pressure generated within the discharge channels as well as by the rapid cooling of the electrolyte (equation 3). Diffusion of silicate ions through the growing oxide layer and its reaction with the Mg^{2+} ions could be accounted for the formation of Mg_2SiO_4 and $MgSiO_3$ (equations 4-6).

$$Mg \longrightarrow Mg^{2+} + 2e^- \quad \ldots(1)$$

$$Mg^{2+} + 2OH^- \longrightarrow Mg(OH)_2 \quad \ldots(2)$$

$$Mg(OH)_2 \longrightarrow MgO + H_2O \quad \ldots(3)$$

$$2Mg^{2+} + 2SiO_3^{2-} \longrightarrow Mg_2SiO_4 + SiO_2 \quad \ldots(4)$$

$$2Mg^{2+} + SiO_3^{2-} + 2OH^- \longrightarrow Mg_2SiO_4 + H_2O \quad \ldots(5)$$

$$Mg^{2+} + SiO_3^{2-} \longrightarrow MgSiO_3 \quad \ldots(6)$$

Alkaline post-treatment of PEO coated Mg using 3 M NaOH at 60 °C for 1 h has led to modification of the porous structure with a fine spherical or globular feature (Fig. 1(c)). Alkaline treatment of Mg and its alloys often leads to the formation of $Mg(OH)_2$ due to its low free energy of formation (-833.7 kJ/mol) and poor solubility product (K_{sp}: 1.5×10^{-11}). $Mg(OH)_2$ has a layered structure wherein the Mg^{2+} ions are arranged in the form of a hexagonal layer while the OH^- ions constitute similar layers above and below, thus resulting in platelet-shaped crystals.[23-25] However, depending on the method of synthesis employed, $Mg(OH)_2$ could adopt needle-like, lamellar-like, wire-like, rod-like and flower-like morphologies.[26-34] According to Lv et al.[28] and Khanjani et al.,[35] alkali concentration is the prime factor in determining the morphology of $Mg(OH)_2$ crystals. In the present study, 3 M NaOH is used for post-treatment of the PEO coated Mg. The higher concentration of OH^- ions is likely to favour a high supersaturation level, thus promoting nucleation of the $Mg(OH)_2$ crystals. The isoelectric point of $Mg(OH)_2$ is 12.[36] Since the pH of 3 M NaOH is >13, the $Mg(OH)_2$ crystals would assume a net negative charge. The presence of a higher concentration of Na^+ ions with a small hydration sphere and a positive charge could facilitate their preferential adsorption on the growing $Mg(OH)_2$ nuclei over the Mg^{2+} ions. To reduce the surface energy they could agglomerate, thus resulting in fine spherical or globular feature.[37]

A closer look at the morphology of the PEO coated Mg after alkaline post-treatment reveals that the spherical or globular feature is developed around the pores and it effectively seals the smaller pores besides reducing the diameter of medium and large sized pores to ~ 0.45 μm and ~0.75 μm, respectively (Fig. 1(d)). In order to make a quantitative comparison of the pore density, the FE-SEM images shown in Figs. 1 (a) and 1(c) are subjected to image processing and the processed images are shown in Figs. 1(e) and 1(f), respectively. The pore pixels are represented by black colour while the background is outlined by green colour. A comparison of the processed images shown in Figs. 1(e) and 1(f)

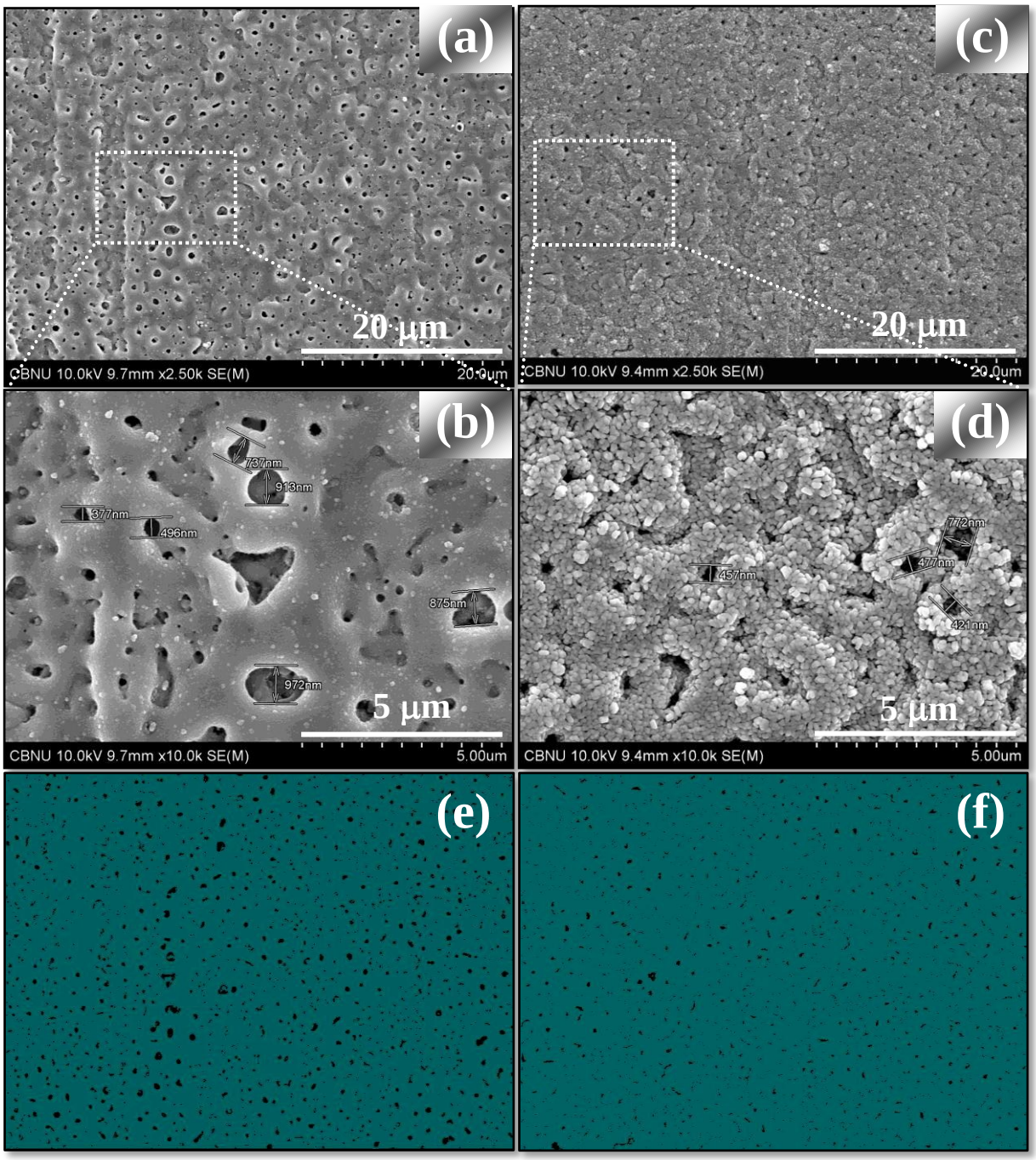

Fig. 1 Surface morphology of (a, b) PEO coated Mg; and (c, d) PEO coated Mg post-treated using 3 M NaOH at 60 °C for 1 h; (e, f) Processed images acquired after image processing of the FE-SEM images shown in (a) and (d), respectively, that provides a comparison of pore size and pore density of the PEO coated Mg before and after alkaline post-treatment

Table 1 Chemical composition of the PEO coating before and after alkaline post-treatment

Analysis area	Elemental concentration (in at. %)			
	O	Mg	Si	Na
Over the entire area of the coating shown on Fig. 1(a)	38.86	46.99	14.15	-
Over the entire area of the coating shown on Fig. 1(d)	39.36	46.69	12.03	1.93

clearly reveals a decrease in average pore size and density after alkaline post-treatment. Quantitative calculation shows a reduction in pore density from 296 pixels/mm^2 (before treatment) to 156 pixels /mm^2 after alkaline post-treatment using 3 M NaOH.

This leads to the question that will it be possible to reduce the pore density of the PEO coatings by directly adding $Mg(OH)_2$ to the electrolyte used for PEO? Addition of $Sr(OH)_2$ in electrolytes used for PEO, in the range of 0.0013 to 0.013 M, fails to exhibit any major change in the porous structure of the resultant coatings.[38, 39] The characteristics of PEO coatings prepared using 0.09 M and 0.27 M KOH was studied earlier by Ko et al.[40] An increase in KOH concentration from 0.09 M to 0.27 M has increased the electrolyte conductivity and enabled the generation of microarcs at a relatively lower voltage. Addition of higher concentrations of $Mg(OH)_2$ in the electrolyte used for PEO is likely to cause similar effects. During PEO, the reaction between Mg^{2+} ions generated at the anode and the OH^- produces $Mg(OH)_2$. However, it is converted to MgO due to the high temperature generated during sparking. Hence, addition of $Mg(OH)_2$ could enhance the volume fraction of the MgO phase. Nevertheless, due to the inherent process features of PEO, the formation of a porous structure could not be avoided. In our earlier work, a duplex treatment combining anodizing and PEO was explored.[41] In one approach, PEO coating (using the same electrolyte and conditions employed in the present study) was deposited on pre-anodized Mg (using 0.3 M NaOH + 15 g/l ZrO_2 particles at 10 V for 30 min) while in the other the anodizing stage was employed as a post-treatment over PEO coated Mg. PEO coating deposited on pre-anodized Mg exhibits a decrease in size and density of the pores. However, the pores of the PEO coating could not be sealed. The anodizing post-treatment of the PEO coated Mg using 0.3 M NaOH based electrolyte has led only to a partial coverage of the pores with lamellar shaped $Mg(OH)_2$. These inferences validate that it is difficult to avoid the porous structure of PEO coating and the importance of the alkaline post-treatment stage using a higher concentration of NaOH explored in the present study. EDAX analysis shows the predominance of O (39.36 at. %), Mg (46.69 at. %) and Si (12.03 at. %) along with a small amount of Na (1.93 at. %) (Table 1). The change in morphology, slight increase in O content (from 38.86 to 39.36 at. %), decrease in Si content (from 14.15 to 12.03 at. %) and the inclusion of Na (1.93 at. %) signify modification of the surface in terms of its coverage, sealing of pores as well as its chemical nature. Dissolution of a fraction of the PEO coating during alkaline post-treatment in 3 M NaOH at 60 °C for 1 h could be possible. The decrease in Si content from 14.15 to 12.03 at. %, suggests such a possibility.

The surface topographic images acquired at a 5 × 5 µm scale over the surface of PEO coated Mg and those post-treated using 3M NaOH at 60 °C for 1 h, along with the parameters of surface roughness, are shown in Fig. 2. The development of fine spherical or globular feature following alkaline post-treatment has led to an increase in the root mean square roughness (R_q) and average surface roughness (R_a). However, the limited increase in the maximum vertical distance between the highest and lowest data points in the image (R_{max}) is due to

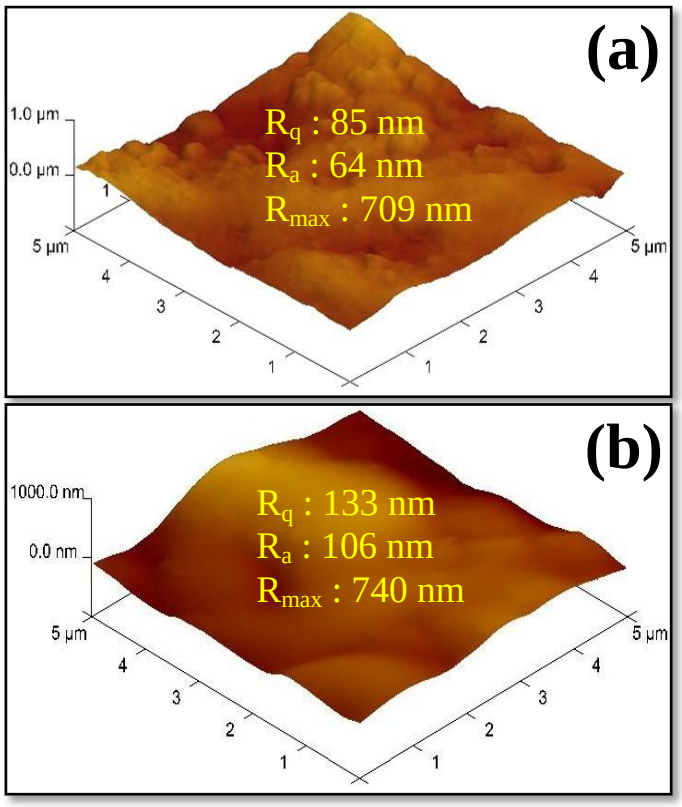

Fig. 2 Surface topographic images and the parameters of surface roughness of (a) PEO coated Mg; and (b) PEO coated Mg post-treated using 3 M NaOH at 60 °C for 1 h (Images are acquired at 5 × 5 µm scale)

the better homogeneity of the globular-like feature all over the surface. An increase in R_q and R_a with better surface homogeneity is considered to be beneficial for better cell proliferation and growth.

The FT-IR spectra of the PEO coated Mg and those post-treated using 3M NaOH at 60 °C for 1 h are traced in Fig. 3. PEO coated Mg shows the presence of four major IR bands at 3419, 1419, 919 and 547 cm^{-1} (curve (a) in Fig. 3). The broad band at 3419 cm^{-1} could be attributed to O-H stretching of H_2O and/or surface adsorbed -OH group. The other broad band observed at 1419 cm^{-1} could be ascribed to antisymmetric stretching vibration of carbonates adsorbed on the surface. The bands at 919 and 547 cm^{-1} could be correlated to Si-O and Mg-O stretching vibrations, respectively. After alkaline post-treatment, formation of new IR bands as well as an increase in intensity of certain bands is observed (curve (b) in Fig. 3). The sharp IR band at 3699 cm^{-1} is characteristic of the O-H stretching vibration of $Mg(OH)_2$. The bands at 3537 and 3472 cm^{-1} represent O-H stretching of H_2O and/or surface adsorbed -OH group while those observed at 1730 and 1647 cm^{-1} correspond to H-O-H bending and rotation of H_2O. As already mentioned, the bands at 1404, 928 and 547 cm^{-1} represent antisymmetric stretching of carbonates adsorbed on the surface, Si-O stretching and Mg-O stretching vibrations, respectively. The newly formed sharp band at 3699 cm^{-1} along with the increase in intensity of bands at 1404, 928 and

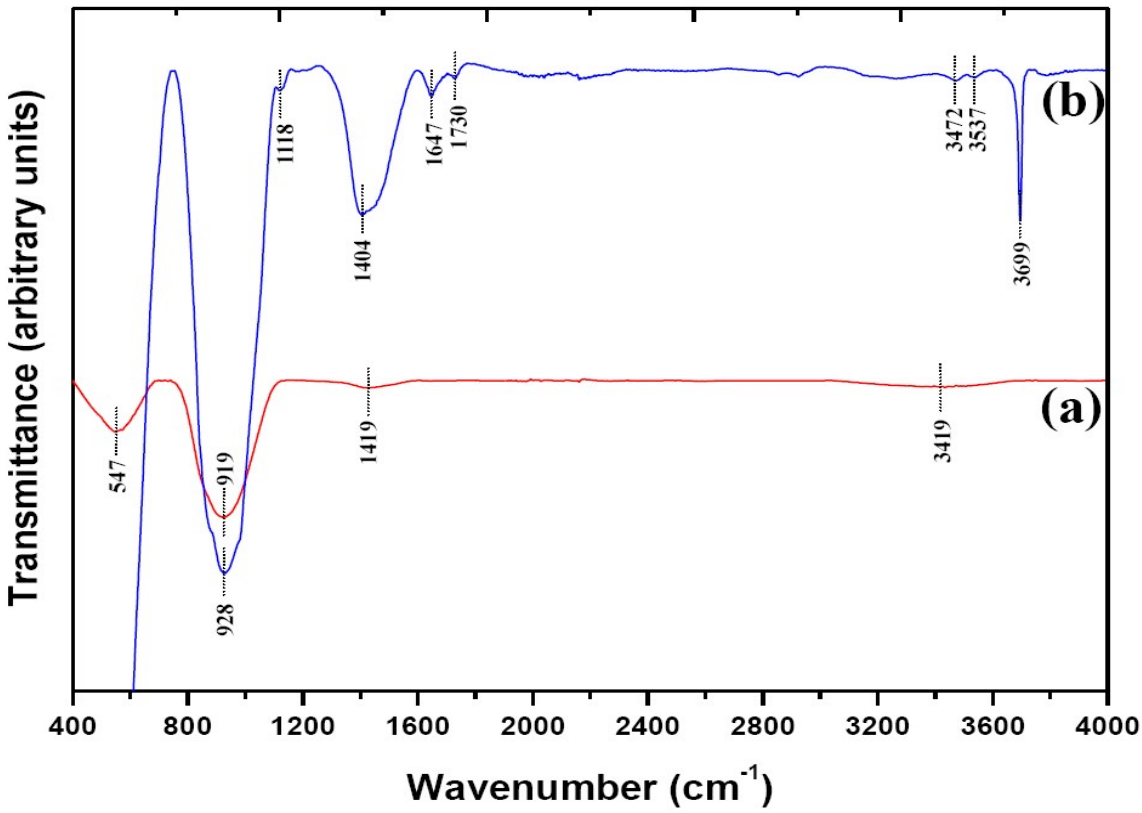

Fig. 3 Comparison of the FT-IR spectra of (a) PEO coating deposited on Mg using alkaline silicate electrolyte at 250 V for 2 min; and (b) PEO coated Mg post-treated using 3 M NaOH at 60 °C for 1 h

547 cm^{-1} confirms modification of the surface after alkaline post-treatment in terms of its chemical nature.

The TF-XRD patterns of PEO coating deposited on Mg and those subjected to alkaline post-treatment are shown in Fig. 4. Formation of MgO, Mg_2SiO_4 and $MgSiO_3$ phases are evident on PEO coated Mg (curve (a) in Fig. 4). Besides these phases, the formation of $Mg(OH)_2$ and $((Mg_2SiO_4)_2)((Mg(OH)_2)_3)$ could be observed on PEO coated Mg post-treated using 3 M NaOH (curve (b) in Fig. 4). The formation of $Mg(OH)_2$ is also confirmed by the sharp band observed at 3699 cm^{-1} in the FT-IR spectrum (curve (b) in Fig. 3). It is obvious to expect the formation of $Mg(OH)_2$ during alkaline post-treatment. The formation of $((Mg_2SiO_4)_2)((Mg(OH)_2)_3)$, referred as magnesium hydroxide silicate, is identified for the first time in this study. The formation of this phase along with a decrease in Si content from 14.15 to 12.03 at. % following alkaline post-treatment indicates the involvement of a direct reaction between Mg_2SiO_4 and $MgSiO_3$ with NaOH, which could have accompanied by the dissolution of a fraction of the PEO coating. The dissolution and reprecipitation process could have enabled the spherical morphological feature (Figs. 1(d) and 1(e)).

The polarization curves of uncoated Mg, PEO coated Mg and PEO coated Mg post-treated using 3 M NaOH, in HBSS, are shown in Fig. 5. The corrosion potential (E_{corr}) and corrosion current density (i_{corr}), provides the basis for ranking their corrosion protective ability. The E_{corr} of uncoated Mg, PEO coated Mg and PEO coated Mg post-treated using 3 M NaOH are -1.54 V, -1.47 V and -1.58 V vs. Ag/AgCl/KCl (sat.), respectively while the corresponding i_{corr} are 1.38 x 10^{-5}, 1.70 x 10^{-6} and 4.42 x 10^{-7} A/cm^2, respectively. It is evident that post-treatment of PEO coated Mg using 3 M NaOH at 60 °C for 1 h has led to an improvement in corrosion resistance when compared to the as-deposited PEO coated Mg. Immersion in HBSS at 37 °C for 168 h provides a useful measure of the ability of the coated Mg to offer long-term corrosion protection. The change in pH of HBSS as a function of immersion time is shown in Fig. 6. During corrosion, dissolution of Mg (equation 7) is accompanied by reduction of water (equation 8), which is responsible for the observed increase in pH (Fig. 6). The increase in pH is rapid during the first 8 to 12 h. However with a further increase in immersion time, the rate of increase in pH is decreased considerably. This is due to the formation of $Mg(OH)_2$ (equation 9), which covers the surface. However, the porous nature of the $Mg(OH)_2$ layer allows permeation of HBSS that enables further dissolution of Mg through them and an increase in pH. Dissolution of $Mg(OH)_2$ (equation 10) by the Cl^- ions present in HBSS prevents the barrier layer effect caused by them.[42, 43]

$$Mg \longrightarrow Mg^{2+} + 2e^- \quad \ldots(7)$$

$$2H_2O + 2e^- \longrightarrow H_2\uparrow + 2OH^- \quad \ldots(8)$$

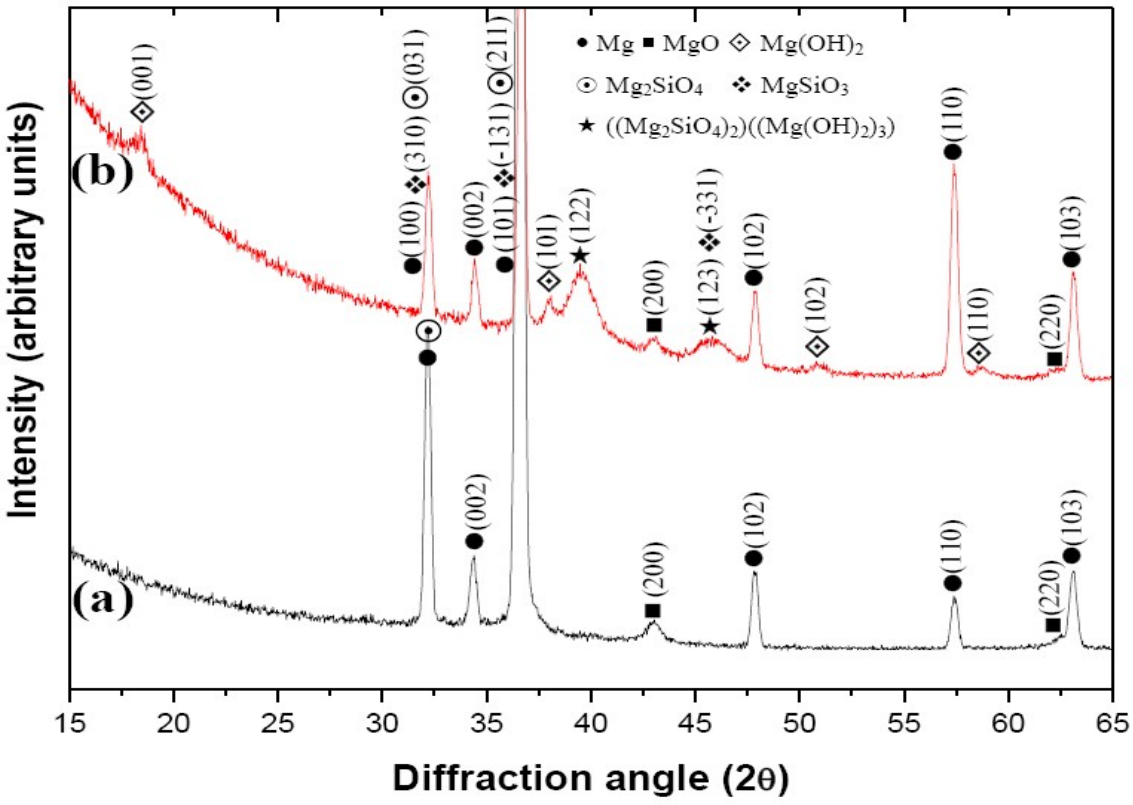

Fig. 4 TF-XRD patterns of (a) PEO coating deposited on Mg using alkaline silicate electrolyte at 250 V for 2 min; and (b) PEO coated Mg post-treated using 3 M NaOH at 60 °C for 1 h

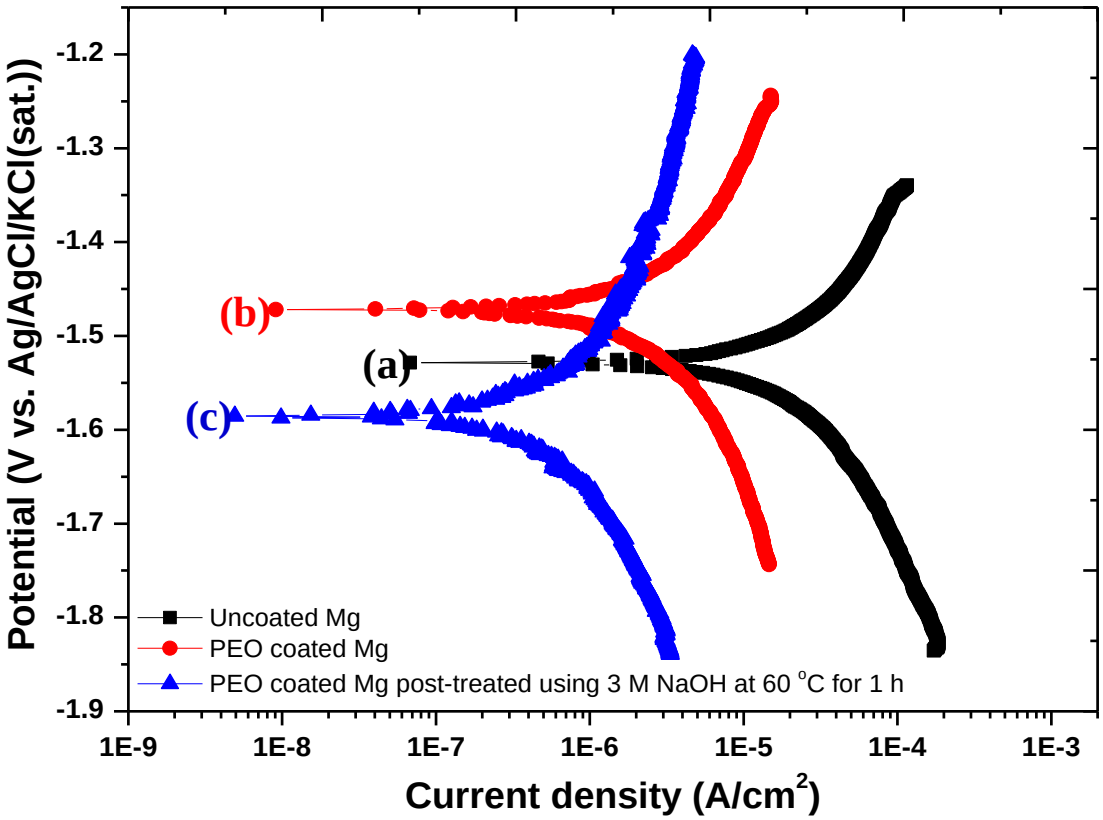

Fig. 5 Potentiodynamic polarization curves of (a) untreated Mg; (b) PEO coated Mg; and (c) PEO coated Mg post-treated using 3 M NaOH at 60 °C for 1 h, in HBSS

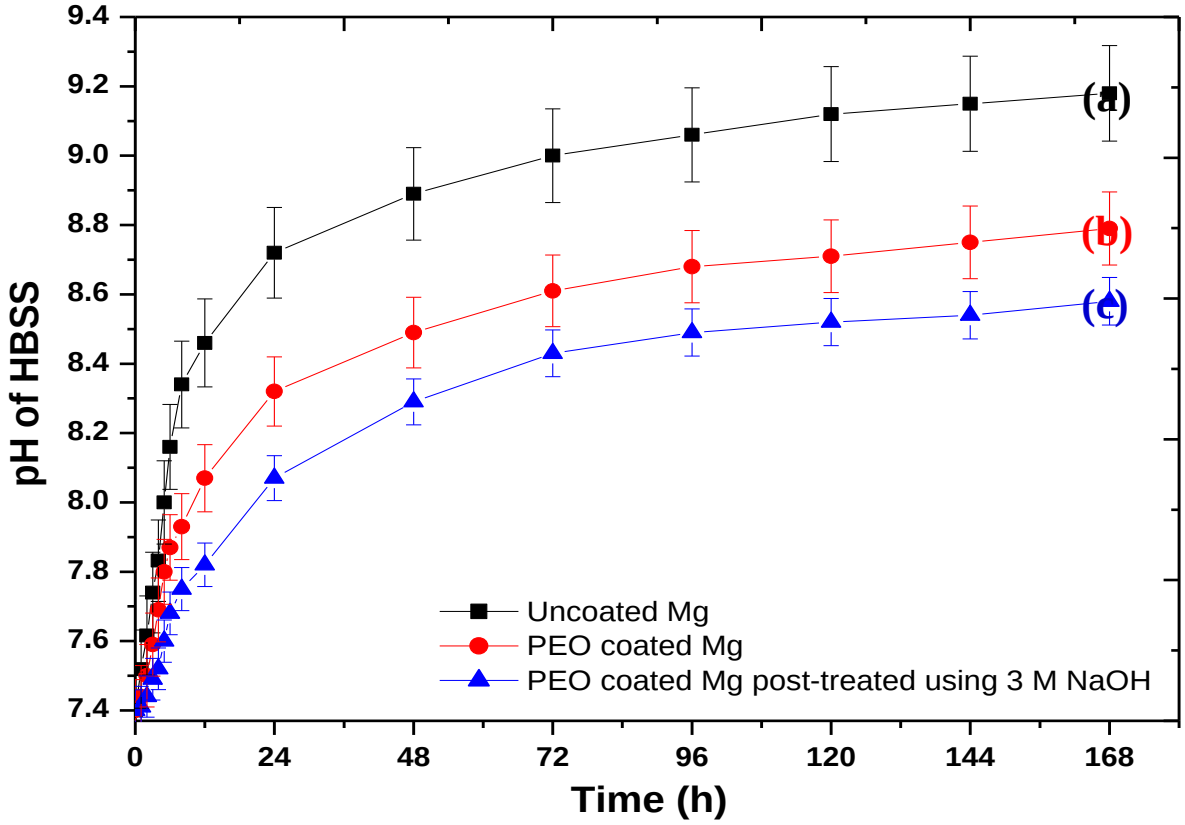

Fig. 6 Extent of change in pH of HBSS during corrosion of (a) untreated Mg; (b) PEO coated Mg; and (c) PEO coated Mg post-treated using 3 M NaOH at 60 °C for 1 h, measured as a function of immersion time

$$Mg^{2+} + 2OH^- \longrightarrow Mg(OH)_2 \downarrow \quad ...(9)$$

$$Mg(OH)_2 + 2Cl^- \longrightarrow MgCl_2 + 2OH^- \quad ...(10)$$

The pH of HBSS reached a stable value after a prolonged immersion time. This suggests establishment of equilibrium between the rate of formation and dissolution of corrosion products. It is evident from Fig. 6 that the trend is similar for both untreated and PEO coated Mg with and without post-treatment. However, the extent and rate of change in pH is relatively less for the PEO coated ones than the uncoated Mg. The extent of corrosion attack of uncoated Mg, PEO coated Mg and PEO coated Mg post-treated using 3 M NaOH, after immersion in HBSS at 37 °C for 168 h and after removal of the corrosion products, is shown in Fig. 7. All of them exhibit localized corrosion attack. This is due to the presence of higher concentrations of Cl^- ions in HBSS that attack Mg specifically at the defect site.[44] The extent of corrosion damage is severe on uncoated Mg than on the PEO coated ones. Based on the i_{corr} value derived from the potentiodynamic polarization study (Fig. 5), rate and extent of change in pH measured as a function of time in HBSS (Fig. 6) and the extent of localized corrosion attack after 168 h of immersion in HBSS (Fig. 7), it is clear that PEO coated Mg post-treated using 3 M NaOH exhibits a better corrosion protective ability than the PEO coated Mg and the uncoated one. The observed improvement in corrosion resistance of PEO coated Mg post-treated using 3 M NaOH is due to the modified surface with a spherical or globular morphology that covered the small size pores and decreased the diameter of the medium and large size pores. The hindrance in permeation of HBSS to the base metal following the decrease in porosity is considered as the main reason for the observed improvement in corrosion resistance. Formation of $((Mg_2SiO_4)_2)((Mg(OH)_2)_3)$ is very specific to the PEO coated Mg post-treated using 3 M NaOH. The contribution of this phase towards corrosion resistance is not clear and warrants further study.

The surface morphology of uncoated Mg, PEO coated Mg and PEO coated Mg post-treated using 3 M NaOH after immersion in SBF at 37 °C for 240 h is shown in Fig. 8. The formation of corrosion products could be observed on the surface of all the samples. The corrosion product layer is reasonably thick that neither the porous structure of PEO coated Mg nor the modified structure of PEO coated Mg post-treated using 3 M NaOH could be observed. A typical “mudcrack” pattern is observed on all samples. These cracks could have formed due to the dehydration and shrinkage of the surface layer during drying in air as well when the samples are placed in vacuum atmosphere as during FE-SEM analysis. It is interesting to note that the PEO coated Mg post-treated using 3 M NaOH is covered with spherical or granular precipitates all over the surface whereas such features are relatively less over PEO coated Mg while it is rather limited on the surface of uncoated Mg. EDAX analysis performed over the entire area of the surface layer shown in Figs. 8(a)-8(c) reveals the presence of O, Mg, Ca and P as

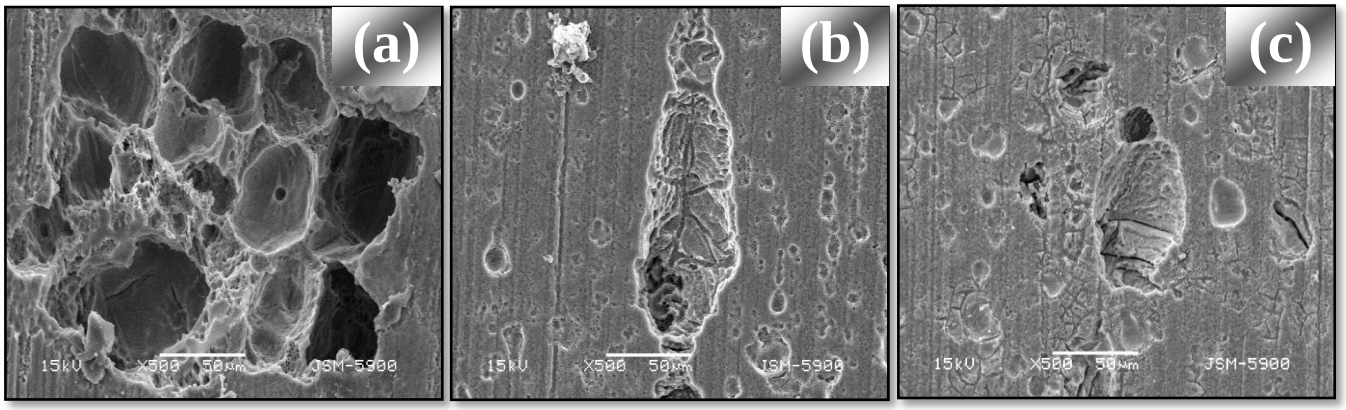

Fig. 7 Extent of corrosion attack of (a) untreated Mg; (b) PEO coated Mg; and (c) PEO coated Mg post-treated using 3 M NaOH at 60 °C for 1 h, after immersion in HBSS at 37 °C for 168 h and after removal of the corrosion products

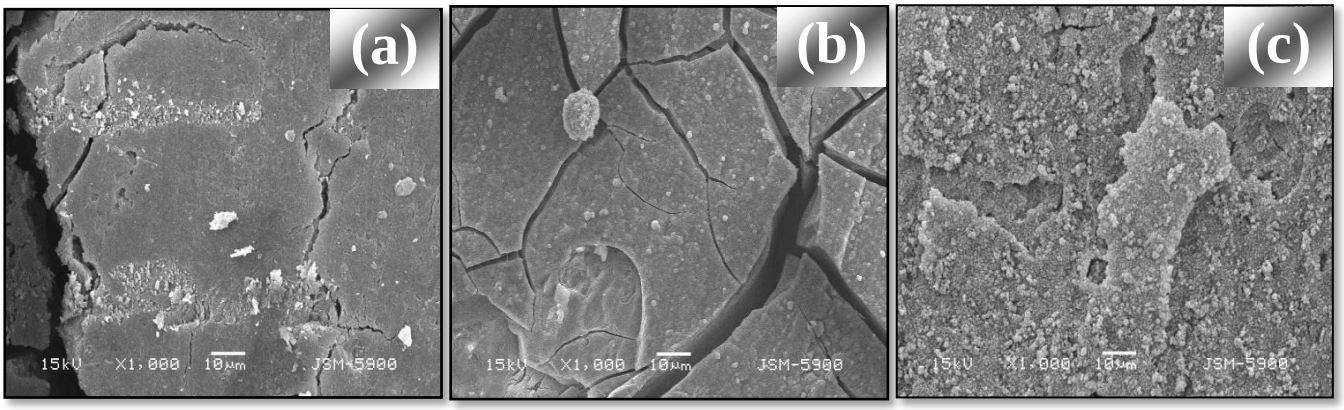

Fig. 8 Morphological features of the surface layer formed on (a) untreated Mg; (b) PEO coated Mg; and (c) PEO coated Mg post-treated using 3 M NaOH at 60 °C for 1 h, after immersion in SBF at 37 °C for 240 h

major elements along with a small amount of Si (Table 2). The presence of Mg and O suggests the possibility of formation of $Mg(OH)_2$, the mechanism of which is already explained (equations 7, 8 and 9). The OH^- ions generated following the reduction of water (equation 8) could lead to reduction of $H_2PO_4^-$ and HPO_4^{2-} ions (equations 11 and 12).

$$H_2PO_4^- + 2OH^- \longrightarrow PO_4^{3-} + 2H_2O \quad \ldots(11)$$

$$2HPO_4^{2-} + 2OH^- \longrightarrow 2PO_4^{3-} + 2H_2O \quad \ldots(12)$$

The PO_4^{3-} ions could combine with both Ca^{2+} and Mg^{2+} ions, leading to the formation of calcium and magnesium phosphates, which correlates well with the presence of Ca, Mg, P and O in the EDAX analysis (Table 2). Based on the low solubility constant (K_{sp}), formation of $Ca_{10}(PO_4)_6(OH)_2$ (K_{sp}: 1.6×10^{-58}) and $Mg_3(PO_4)_2$ (K_{sp}: 1.04×10^{-24}) are considered as most probable. The formation of $Mg(OH)_2$ as a major compound along with calcium and magnesium phosphates has also been previously reported during corrosion of Mg alloys in SBF.[42-44] According to Rabadjieva et al.,[45] when the pH of the SBF ranges between 8 and 11.50, formation of an amorphous calcium phosphate phase ($Ca_3(PO_4)_2.3H_2O$) is kinetically favoured than the thermodynamically more stable hydroxyapatite phase. Kuwahara.[46] also observed the formation of $(Ca_{0.86}Mg_{0.14})_{10}(PO_4)_6(OH)_2$ during corrosion of Mg in SBF. It is evident from the EDAX analysis that the Ca and P contents are relatively high in the surface layer formed over PEO coated Mg post-treated using 3 M NaOH when compared to the others (Table 2). The relatively lower amount of Ca than P indicates the formation of calcium deficient apatites on all the samples. Zhao et al.[47] have also observed the formation of calcium deficient apatites when MAO coated Mg is immersed in SBF at 37 °C for 168 h. Since calcium deficient apatites have the ability to induce new bone like apatites,[48] their formation assumes significance. The appearance of spherical or granular precipitates all over the surface as well as a relatively higher Ca and P contents signify a relatively higher extent of apatite formation over the surface of PEO coated Mg post-treated using 3 M NaOH. Since the Na content of the modified layer formed of PEO coated Mg after alkaline post-treatment is only 1.93 at. % (Table 1), the release of Na^+ ions from this layer could not be considered responsible for the higher level of apatite formation. However, the increase in surface roughness and a larger surface area provided by the globular-like feature could have promoted the apatite formation. Anawati et al.[18] have also correlated a larger contact area formed after alkaline post-treatment for the promotion of apatite growth. The higher rate of dissolution of Mg and the inhibition effect of Mg^{2+} ions on the precipitation of apatites[49] could be accounted for the relatively lower extent of apatite formation over uncoated Mg (Fig. 8(a) and Table 2).

Table 2 Chemical composition of the surface layer formed over uncoated Mg, PEO coated Mg and PEO coated Mg post-treated using 3 M NaOH at 60 °C for 1 h, after immersion in SBF at 37 °C for 240 h

Analysis area	Elemental concentration (in at. %)				
	O	Mg	Si	Ca	P
Over the entire area of the coating shown on Fig. 8(a)	70.49	10.18	-	7.14	12.18
Over the entire area of the coating shown on Fig. 8(b)	63.20	12.61	1.01	8.76	14.51
Over the entire area of the coating shown on Fig. 8(c)	61.30	9.73	0.04	13.06	15.10

XRD patterns acquired at the surface layer of uncoated Mg, PEO coated Mg and PEO coated Mg post-treated using 3 M NaOH after immersion in SBF at 37 °C for 240 h reveals the presence of $Mg(OH)_2$ phase (Fig. 9). The broad peak in the diffraction angles between 25 and 35° (marked by dotted rectangle in curve (c) of Fig. 9) is distinct for PEO coated Mg post-treated using 3 M NaOH. This peak could be attributed to the formation of poorly crystalline calcium phosphates. The specific phases of calcium phosphates could not be identified with confidence due to the broadening of the XRD patterns. Li et al.[44] have also reported the difficulty in identifying calcium phosphate other than $Mg(OH)_2$ in the XRD patterns of the recorded on the surface layers formed on pure Mg in SBF's with varying ionic concentrations.

The FT-IR spectra acquired at the surface of uncoated Mg, PEO coated Mg and PEO coated Mg post-treated using 3 M NaOH after immersion in SBF at 37 °C for 240 h is shown in Fig. 10. The sharp peak at ~3698 cm^{-1} could be attributed to the O-H stretching mode, which is typical for the formation of $Mg(OH)_2$. The broad band around 3367-3422 cm^{-1} corresponds to the O-H stretching of H_2O or due to the surface adsorbed -OH group. The IR band observed around 1631-1648 cm^{-1} could be correlated to the H-O-H bending of water. The presence of IR bands pertaining to water confirms that the surface layer formed after immersion in SBF is indeed hydrated and its shrinkage during drying in air and exposure to vacuum atmosphere during FE-SEM analysis has resulted in the formation of cracks. The IR bands at 1023-1048 cm^{-1} corresponds to the P-O stretching of PO_4^{3-} group (v_3 mode). The bands at 556-568 cm^{-1} and those at 430 cm^{-1} corresponds to the O-P-O(H)/O-P bending mode (v_4 mode) and O-P-O bending (v_2 mode) of the PO_4^{3-} group, respectively. The presence of IR bands pertaining to stretching and bending modes of PO_4^{3-} group confirms the formation of phosphates. It has been reported that the formation of IR bands of phosphates at 1040 cm^{-1} and 560 cm^{-1} is associated with the formation of hydroxyapatite.[50-52] SBF is supersaturated with respect to the formation of calcium phosphates. Since the free energy of formation of hydroxyapatite is very low ($\Delta_f G^\circ$ =−6.413 KJ/mol), the probability of its formation is much higher than other phases. The IR bands at 1413-1427 cm^{-1} and 856-866 cm^{-1} could be correlated to the asymmetrical stretching (v_3 mode) and asymmetrical bending (v_2 mode) of CO_3^{2-} group, respectively.[51] The presence of IR bands of CO_3^{2-} group at ~1450 cm^{-1} and at ~875 cm^{-1} along with the phosphate bands at ~1040 cm^{-1} and ~560 cm^{-1} points out a B-type substitution that involves substitution of CO_3^{2-} ions for the PO_4^{3-} ions.[53] This type of substitution is a common phenomenon during precipitation of apatites from biological media, which results in a considerable decrease in crystallinity of the apatite.[51] This inference further validates the poor crystallinity of apatite observed in the XRD patters (Fig. 9).

It is well known that SBF is highly supersaturated that would enable the formation of Ca and P containing apatites.[42] From thermodynamic and kinetic point of view, formation of apatite and its rate of deposition from SBF is promoted by an increase in pH.[19] Corrosion of Mg and the morphological features of the surface layer formed after corrosion confirms the presence of a relatively thick corrosion product (Fig. 8). Hence, the increase in pH during corrosion of Mg could have prompted the precipitation of $Mg(OH)_2$ as well as calcium and magnesium phosphates. The formation of $Mg(OH)_2$ is confirmed by XRD patterns and FT-IR spectra. The presence of peaks pertaining to phosphate is confirmed by FT-IR spectra while the possible precipitation of an amorphous calcium phosphate phase could be observed from the XRD patterns. Based on the surface morphological features (Fig. 8), EDAX analysis (Table 2), XRD patterns (Fig. 9), and the nature of functional groups present in the FT-IR spectra (Fig. 10), it is valid to conclude that the corrosion product layer formed after immersion in SBF is predominantly comprised of $Mg(OH)_2$ and calcium deficient apatites with minor quantities of magnesium phosphate. The inferences made in the study are in line with those observed earlier by other researchers.[54-57] The presence of $((Mg_2SiO_4)_2)((Mg(OH)_2)_3)$ phase, which is very specific to the PEO coated Mg post-treated using 3 M NaOH, did not cause any deleterious influence on the bioactivity in SBF.

Rapid screening of biocompatibility using in vitro cytocompatibility studies is a common procedure followed in the evaluation of biomaterials. Moreover, such methods provide a useful basis for ranking various alloys as well as surface modification methods.[58, 59] Fig. 11 shows the RGR of MC3T3-E1 cells after cell culture using 10% extract of uncoated Mg, PEO coated Mg and PEO coated Mg post-treated using 3 M NaOH, for 1, 2 and 3 days. The RGR of both uncoated as well as PEO coated Mg are > 75% on all the three days. Based on the RGR value, the cytotoxicity of uncoated and PEO coated Mg could be classified as Grade 1 as per ISO 10993-5 standard.

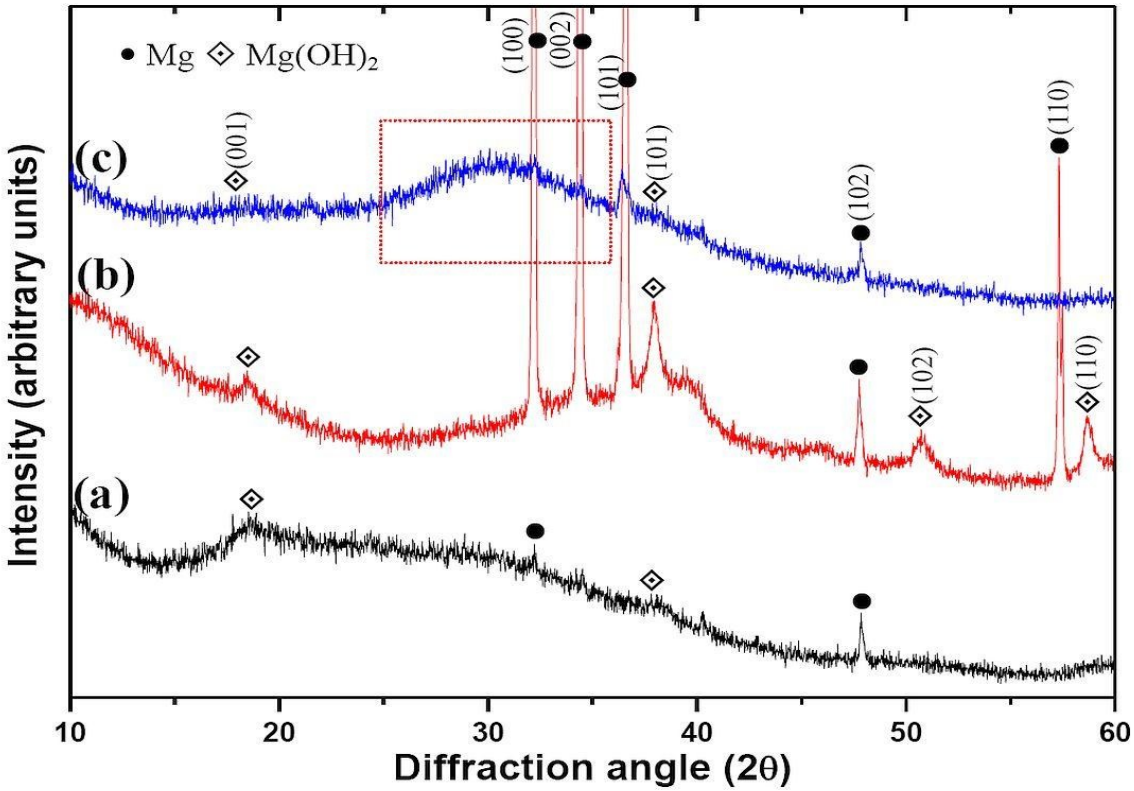

Fig. 9 X-ray diffraction pattern recorded on the surface of (a) uncoated Mg; (b) PEO coated Mg; and (c) PEO coated Mg post-treated using 3 M NaOH at 60 °C for 1 h, after immersion in SBF at 37 °C for 240 h

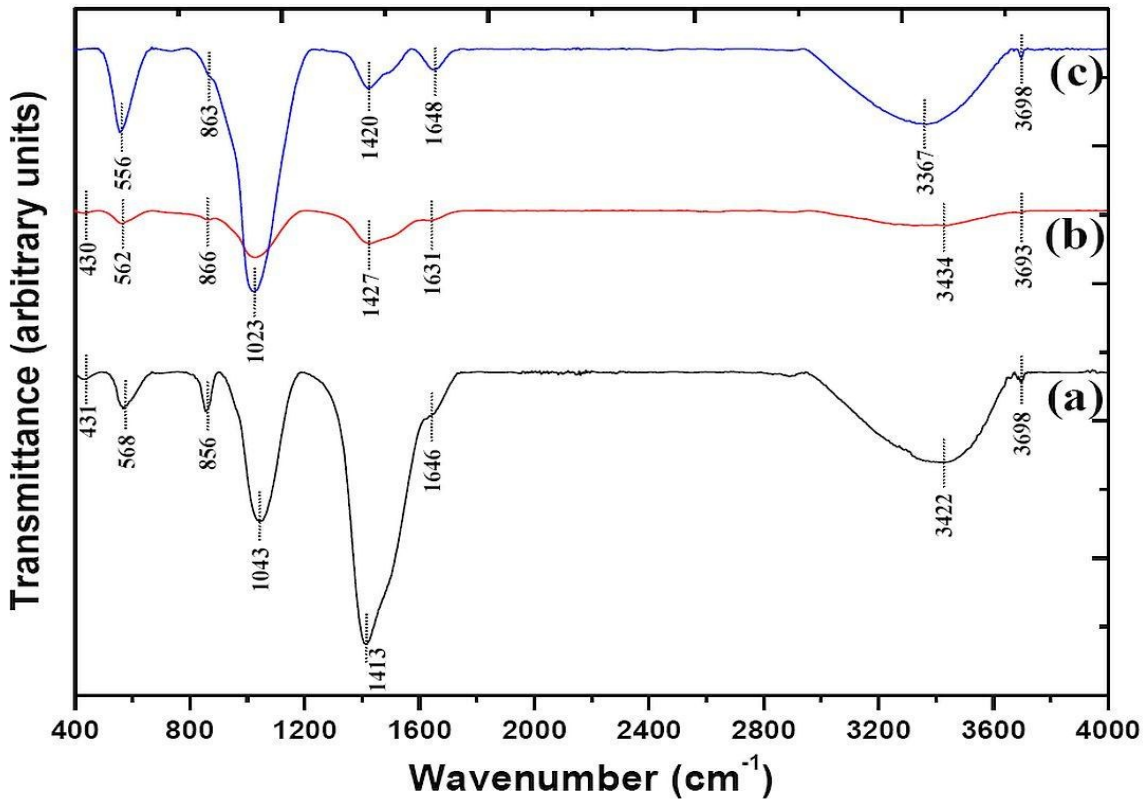

Fig. 10 FT-IR spectra acquired on the surface of (a) uncoated Mg; (b) PEO coated Mg; and (c) PEO coated Mg post-treated using 3 M NaOH at 60 °C for 1 h, after immersion in SBF at 37 °C for 240 h

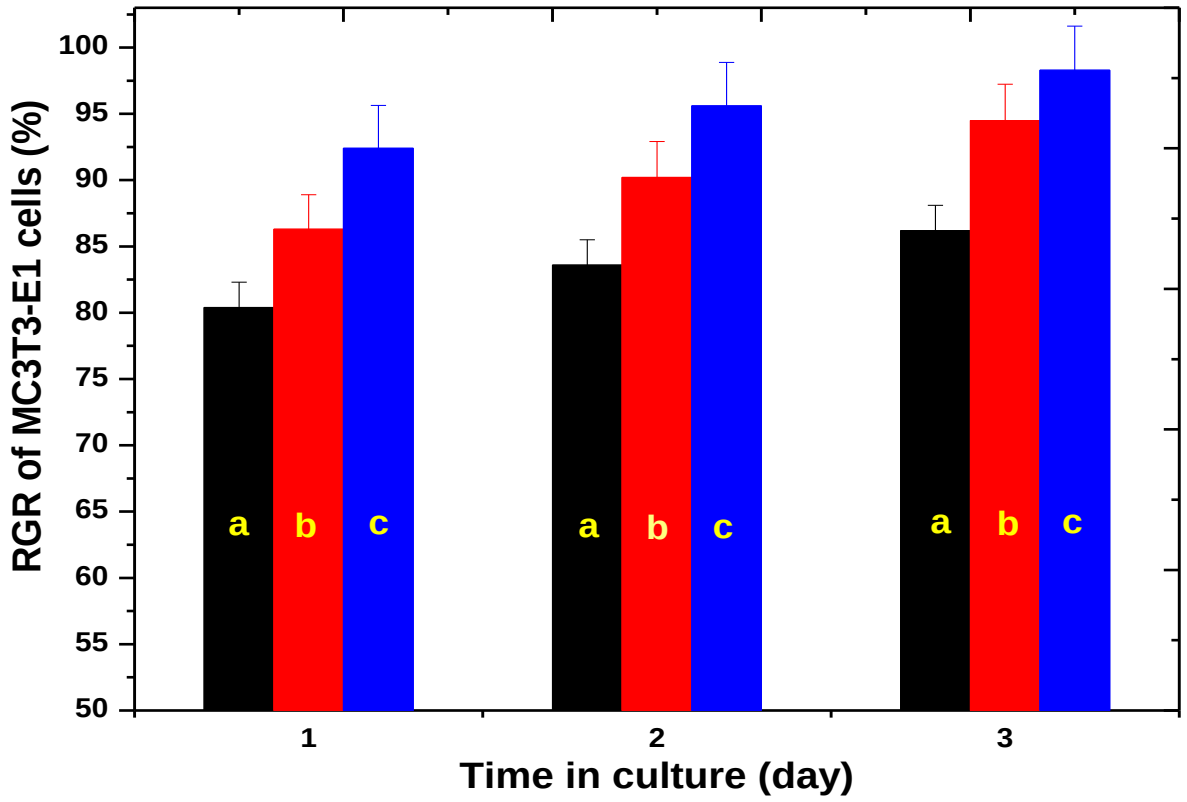

Fig. 11 Relative growth rate (RGR) of MC3T3-E1 cells on (a) uncoated Mg; (b) PEO coated Mg; and (c) PEO coated Mg post-treated using 3 M NaOH at 60 °C for 1 h, after cell culture using 10% extracts for 1, 2 and 3 days

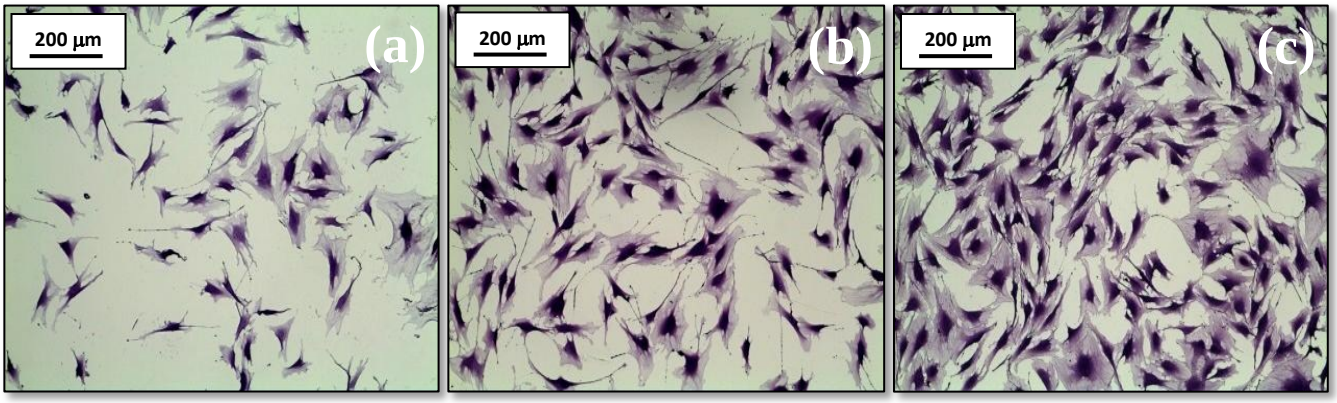

Fig. 12 Cell morphology and the extent of cell growth on (a) uncoated Mg; (b) PEO coated Mg; and (c) PEO coated Mg post-treated using 3 M NaOH at 60 °C for 1 h, after cell culture for 1 day using the 10% extract

The relatively lower RGR value observed for uncoated Mg suggests lower cell viability when compared to the PEO coated ones. This could be due to the relatively higher corrosion rate of uncoated Mg than the PEO coated ones in the cell culture medium. A higher corrosion rate signifies an increase in concentration of Mg^{2+} ions, which could change the osmolality of the cell culture medium leading to rupture of cell membranes and cell death.[60] Moreover, higher concentration of Mg^{2+} ions is likely to deleteriously influence the biological effect of Ca^{2+} ions.[61] Jung et al.[59] have identified the existence of a good correlation between higher corrosion rate of pure Mg as well as untreated WE43 Mg alloy with their poor cytocompatibility. Zhen et al.[62] have suggested that the higher concentration of Mg^{2+} ions demonstrate a strong influence towards the cytotoxicity of Mg alloys while only a weak influence is exerted by the change in pH of the medium. The cell morphology and the extent of cell growth after cell culture for 1 day using the 10% extract is shown in Fig. 12. It is evident that the cell growth is relatively much better on PEO coated Mg post-treated using 3 M NaOH than the PEO coated Mg and the uncoated one. Hence, it is clear that the presence of $((Mg_2SiO_4)_2)((Mg(OH)_2)_3)$ phase, which is very specific to the PEO

coated Mg post-treated using 3 M NaOH, did not cause any deleterious influence on the cytocompatibility in cell culture medium.

In order to get a better insight, the morphology (Fig. 13), chemical composition (Table 3) and FT-IR spectra (Fig. 14) of the surface layer formed on uncoated Mg, PEO coated Mg and PEO coated Mg post-treated using 3 M NaOH after 72 h of immersion in cell culture medium under physiological conditions are acquired. The morphological features of the surface layer resemble those observed after immersion o these samples in SBF for 240 h in terms of formation of a reasonably thick corrosion layer with cracks covering the porous structure of PEO coated Mg. The relatively larger fraction of spherical or granular precipitates (Fig. 13(c)), higher amounts of Ca and P (Table 3) and the presence of IR bands pertaining to phosphates validates the ability of PEO coated Mg post-treated using 3 M NaOH to promote a better bioactivity than those observed over PEO coated Mg and uncoated Mg and substantiate the inferences made after immersion of these samples in SBF for 240 h.

Conclusion

Alkaline post-treatment using 3 M NaOH at 60 °C for 1 h is suggested as a simple strategy to modify the porous structure of PEO coated Mg. It modifies the porous structure of PEO coating on Mg with a fine spherical or globular feature, developed around the pores that effectively seal the smaller pores besides reducing the diameter of medium and large sized pores. Quantitative estimation after image processing reveals a decrease in pore density from 296 pixels/mm^2 (before treatment) to 156 pixels/mm^2 after alkaline post-treatment. TF-XRD patterns confirm the formation of $Mg(OH)_2$ and magnesium hydroxide silicate ($(Mg_2SiO_4)_2$)($(Mg(OH)_2)_3$) on PEO coated Mg post-treated using 3 M NaOH besides the MgO, Mg_2SiO_4 and $MgSiO_3$ that are specific to PEO coated Mg. The formation of ($(Mg_2SiO_4)_2$)($(Mg(OH)_2)_3$) is identified for the first time in this study. The formation of this phase along with a decrease in Si content from 14.15 to 12.03 at. % following alkaline post-treatment suggests dissolution of a fraction of the PEO coating. In spite of an increase in R_q and R_a after alkaline post-treatment, the modified surface exhibits a better surface homogeneity. The i_{corr} values derived from potentiodynamic polarization study, rate and extent of change in pH measured as a function of time in HBSS and the extent of localized corrosion attack after 168 h of immersion in HBSS points out the ability of PEO coated Mg post-treated using 3 M NaOH to offer a better corrosion protective ability when compared to PEO coated Mg and the uncoated one. The modified surface with a spherical or globular morphology covered the small size pores and decreased the diameter of the medium and large size pores. The hindrance in permeation of HBSS to the base metal following the decrease in porosity is considered as the main reason for the observed improvement in corrosion resistance. PEO coated Mg post-treated using 3 M NaOH exhibits better bioactivity, which is evidenced by the broad peak in the diffraction angles between 25 and 35° and a relatively higher amount of Ca and P. The corrosion product layer formed after immersion in SBF is predominantly comprised of $Mg(OH)_2$ and calcium deficient apatites with minor quantities of magnesium phosphate. The RGR of both uncoated as well as PEO coated Mg are > 75% on all the three days, meeting Grade 1 specification in terms of cytocompatibility as per ISO 10993-5 standard. The relatively lower RGR value observed for uncoated Mg suggests low cell viability when compared to the PEO coated ones.

Acknowledgements

This work was financially supported by the National Research Foundation of Korea (NRF) grant funded by the Korea government (MSIP) (2011-0028709, 2013R1A1A2012322 & 2014R1A4A1005309) and Regional Strategic Industry project (2013-R0002274). This paper was also supported by the research funds of Chonbuk National University.

Notes and references

1 C. Blawert, S.P. Sah, N. Scharnagl, M.B. Kannan, Plasma electrolytic oxidation/micro-arc oxidation of magnesium and its alloys, Surface modification of magnesium and its alloys for biomedical applications, Vol. 2, T.S.N. Sankara Narayanan, I.S. Park, M.H. Lee (Editors), Woodhead Publishing, UK (Elsevier Science Inc.) 2015, Chapter 8, pp. 193-234.
2 L. Zhang, J. Zhang, C.-F. Chen, Y. Gu, *Corros. Sci.,* 2015, **91**, 7.
3 T.S.N. Sankara Narayanan, I.S. Park, M.H. Lee, *Prog. Mater. Sci.,* 2014, **60**, 1.
4 P. Shi, W.F. Ng, M.H. Wong, F.T. Cheng, *J. Alloys Compd.,* 2009, **469**, 286.
5 W. Shang, B. Chen, X. Shi, Y. Chen, X. Xiao, *J. Alloys Compd.,* 2009, **474**, 541.
6 U. Malayoglu, K.C. Tekin, S. Shrestha, *Surf. Coat. Technol.,* 2010, **205**, 1793.
7 J.H. Gao, X.Y. Shi, B. Yang, S.S. Hou, E.C. Meng, F.X. Guan, S.K. Guan, *J. Mater. Sci. - Mater. Med.,* 2011, **22**, 1681.
8 M. Laleh, F. Kargar, A. Sabour Rouhaghdam, *J. Sol-Gel Sci. Technol.,* 2011, **59**, 297.
9 Z. Li, X. Jing, Y. Yuan, M. Zhang, *Corros. Sci.,* 2012, **63**, 358.
10 M. Guo, L. Cao, P. Lu, Y. Liu, X. Xu, *J. Mater. Sci. - Mater. Med.,* 2011, **22**, 1735.
11 P. Lu, L. Cao, Y. Lin, X. Xu, X. Wu, *J. Biomed. Mater. Res. B,* 2011, **96,** 101.
12 L.H. Li, T.S.N. Sankara Narayanan, Y.K. Kim, Y.-M. Kong, I.S. Park, T.S. Bae, M.H. Lee, *Thin Solid Films*, 2014, **562**, 561.
13 N.J. Ostrowski, B. Lee, A. Roy, M. Ramanathan, P.N. Kumta, *J. Mater. Sci. Mater. Med.,* 2013, **24**, 85.
14 H.M. Kim, H. Takadama, T. Kokubo, S. Nishiguchi, T. Nakamura, *Biomaterials*, 2000, **21**, 353.
15 V. Jokanović, M. Vilotijević, B. Jokanović, M. Jenko, I. Anžel, D. Stamenković, V. Lazic, R. Rudolf, *Corros. Sci.,* 2014, **82**, 180.
16 J. Waterman, A. Pietak, N. Birbilis, T. Woodfield, G. Dias, M.P. Staiger, *Mater. Sci. Eng. B-Adv.,* 2011, **176**, 1756.

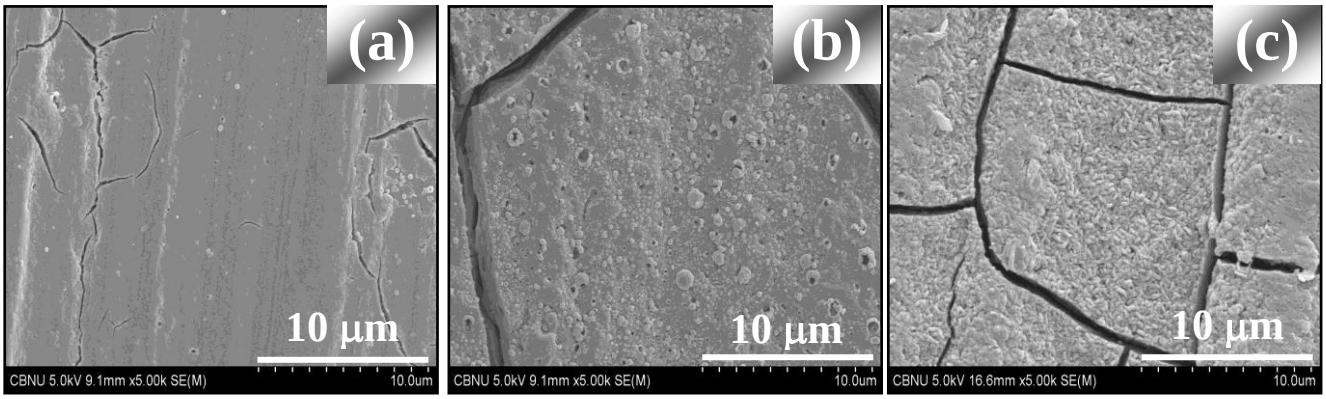

Fig. 13 Morphological features of the surface layer formed on (a) untreated Mg; (b) PEO coated Mg; and (c) PEO coated Mg post-treated using 3 M NaOH at 60 °C for 1 h, after immersion in cell culture medium at 37 °C, 5 % CO_2, 95% relative humidity for 72 h

Table 3 Chemical composition of the surface layer formed over uncoated Mg, PEO coated Mg and PEO coated Mg post-treated using 3 M NaOH at 60 °C for 1 h, after immersion in cell culture medium at 37 °C, 5 % CO_2, 95% relative humidity for 72 h

Analysis area	Elemental concentration (in at. %)				
	O	Mg	Si	Ca	P
Over the entire area of the coating shown on Fig. 11(a)	58.81	30.79	-	3.81	6.59
Over the entire area of the coating shown on Fig. 11(b)	64.95	15.73	1.68	9.48	8.16
Over the entire area of the coating shown on Fig. 11(c)	68.98	5.43	0.36	14.16	11.08

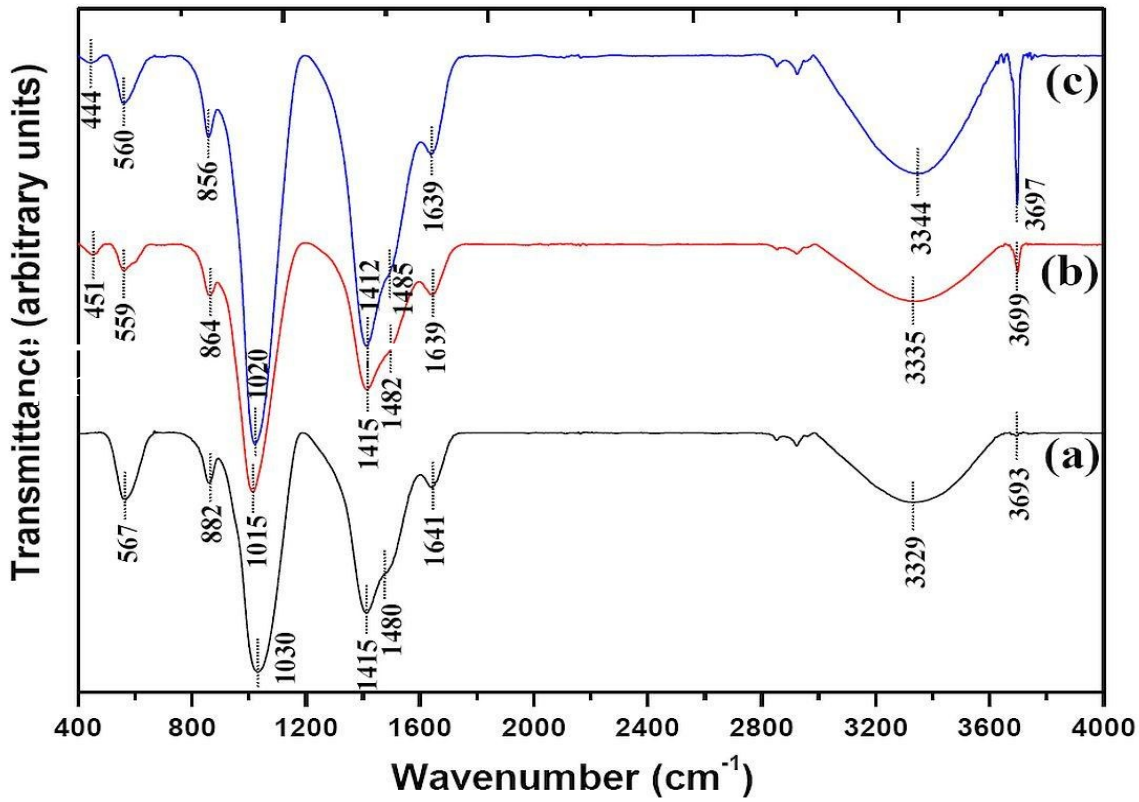

Fig. 14 FT-IR spectra acquired on the surface of (a) Uncoated Mg; (b) PEO coated Mg; and (c) PEO coated Mg post-treated using 3 M NaOH at 60 °C for 1 h, after immersion in cell culture medium at 37 °C, 5 % CO2, 95% relative humidity for 72 h

17 Y. Zhu, G. Wu, Y.-H. Zhang, Q. Zhao, *Appl. Surf. Sci.,* 2011, **257**, 6129.
18 Anawati, H. Asoha, S. Ono, *Surf. Coat. Technol.,* 2015, **272**, 182.
19 X. Lu, Y. Leng, *Biomaterials*, 2005, **26**, 1097.
20 M. Li, J. Liu, J. Li, Y. Li, S. Lu, Y. Yuan, *Prog. Nat. Sci. - Mater. Int.,* 2014, **24**, 486.
21 T.S.N. Sankara Narayanan, I.S. Park, M.H. Lee, *J. Mater. Chem. B,* 2014, **2**, 3365.
22 R.O. Hussein, X. Nie, D.O. Northwood, *Electrochim. Acta,* 2013, **112**, 111.
23 H.R. Oswald, R. Asper, Bivalent metal hydroxides, in: R.M.A. Kieth (Ed.), Physics and Chemistry of Mineral with Layered Structures, vol. 1, Reidel, Dordrecht, 1977.
24 M. Turek, W. Gnot, *Ind. Eng. Chem. Res.*, 1995, **34**, 244.
25 L. Desgranges, G. Calvarin, G. Chevrjier, *Acta Cryst. B,* 1996, **52**, 82.
26 Y. Li, M. Sui, Y. Ding, G. Zhang, J. Zhuang, C. Wang, *Adv. Mater.,* 2000, **12**, 818.
27 Y. Ding, G. Zhang, H. Wu, B. Hai, L. Wang, Y. Qian, *Chem. Mater.,* 2001, **13**, 435.
28 J. Lv, L. Qiu, B. Qu, *J. Cryst. Growth,* 2004, **267**, 676.
29 J.C. Yu, A. Xu, L. Zhang, R. Song, L. Wu, *J. Phys. Chem. B,* 2004, **108**, 64.
30 C. Yan, D. Xue, L. Zou, X. Yan, W.Wang, *J. Cryst. Growth,* 2005, **282**, 448.
31 K.T. Ranjit, K.J. Klabunde, *Langmuir,* 2005, **21**, 12386.
32 J.-P. Hsu, A. Nacu, *Colloid Surface A,* 2005, **262**, 220.
33 Y. Gao, H. Wang, Y.L. Su, Q. Shen, D. Wang, *J. Cryst. Growth,* 2008, **310**, 3771.
34 G. Zou, W. Chen, R. Liu, Z. Xu, *Mater. Chem. Phys.,* 2008, **107**, 85.
35 S. Khanjani, A. Morsali, *Ultrason. Sonochem.,* 2013, **20**, 729.
36 T. X. Phuoc, B.H. Howard, D.V. Martello, Y. Soong, M.K. Chyu, *Opt. Lasers Eng.,* 2008, **46**, 829.
37 C. Henrista, J.P. Mathieua, C. Vogelsb, A. Rulmonta, R. Cloots, *J. Cryst. Growth,* 2003, **249**, 321.
38 K.-C. Kung, T.-M. Lee, T.-S. Lui, *J. Alloys Compd.,* 2010, **508**, 384.
39 X. Lin, X. Yang, L. Tan, M. Lic, X. Wang, Y. Zhang, K. Yang, Z. Hu, J. Qiu, *Appl. Surf. Sci.,* 2014, **288**, 718.
40 Y.G. Ko, S. Namgung, D.H. Shin, *Surf. Coat. Technol.,* 2010, **205**, 2525.
41 T.S.N. Sankara Narayanan, Min Ho Lee, *J. Colloid Interface Sci.,* 2016, **464**, 36.
42 Y. Song, D. Shan, R. Chen, F. Zhang, E.H. Han, *Mater. Sci. Eng. C*, 2009, **29**, 1039.
43 M.I. Jamesh, G. Wu, Y. Zhao, D.R. McKenzie, M.M.M. Bilek, P.K. Chu, Corros. Sci., 2015, **91**, 160.
44 Z. Li, G.-L. Song, S. Song, *Electrochim. Acta*, 2014, **115**, 56.
45 D. Rabadjieva, R. Gergulova, R. Titorenkova, S. Tepavitcharova, E. Dyulgerova, Chr. Balarew, O. Petrov, *J. Mater. Sci. Mater. Med.,* 2010, **21**, 2501.
46 H. Kuwahara, Y. Al-Abdullat, N. Mazaki, S. Tsutsumi, T. Aizawa, *Mater. Trans.,* 2001, **42**, 1317.
47 L. Zhao, C. Cui, X. Wang, S. Liu, S. Bu, Q. Wang, Y. Qi, *Appl. Surf. Sci.,* 2015, **330**, 431.
48 J.H. Gao, S.K. Guan, J. Chen, L.G. Wang, S.J. Zhu, J.H. Hu, Z.W. Ren, *Appl. Surf. Sci.,* 2011, **257**, 2231.
49 M. Hermassi, C. Valderrama, J. Dosta, J.L. Cortina, N.H. Batis, *Chem. Eng. J.,* 2016, **283**, 572.
50 M.R. Filgueiras, G. LaTorre, L.L. Hench, *J. Biomed. Mater. Res.,* 1993, **27**, 445.
51 N. Patel, S.M. Best, W.J. Bonfield, J. Aust. Ceram. Soc., 2005; **41**, 1.
52 W. Xiao, B.S. Bal, M.N. Rahaman, *Mater. Sci. Eng. C,* 2016, **60**, 324.
53 R.Z. LeGeros, J.P. LeGeros, R.O. Trautz, E. Klein, *Dev. Appl. Spectrosc.*, 1970, **7B**, 12.
54 F. Witte, V. Kaese, H. Haferkamp, E. Switzer, A. Meyer-Lindenberg, C.J. Wirth, H. Windhagen, *Biomaterials*, 2005, **26**, 3557.
55 R. Rettig, S. Virtanen, *J. Biomed. Mater. Res. A*, 2009, **88**, 359.
56 M. Ascencio, M. Pekguleryuz, S. Omanovic, *Corros. Sci.,* 2014, **87**, 489.
57 M. Ascencio, M. Pekguleryuz, S. Omanovic, *Corros. Sci.,* 2015, **91**, 297.
58 L. Scheideler, C. Füger, C. Schille, F. Rupp, H.-P. Wendel, N. Hort, H.P. Reichel, J. Geis-Gerstorfer, *Acta Biomater.,* 2013, 9, 8740.
59 O. Jung, R. Smeets, D. Porchetta, A. Kopp, C. Ptock, U. Müller, M. Heiland, M. Schwade, B. Behr, N. Kroeger, L. Kluwe, H. Hanken, P. Hartjen, *Acta Biomater.,* 2015, 23, 354.
60 J. Fischer, D. Profrock, N. Hort, R. Willumeit, F. Feyerabend, *Mater. Sci. Eng. B,* 2011, **176**, 1773.
61 B. Zhang, Y. Hou, X. Wang, Y. Wang, L. Geng, *Mater. Sci. Eng. C*, 2011, **31**, 1667.
62 Z. Zhen, X. Liu, T. Huang, T. Xi, Y. Zheng, *Mater. Sci. Eng. C*, 2015, **46**, 202.

Table of content

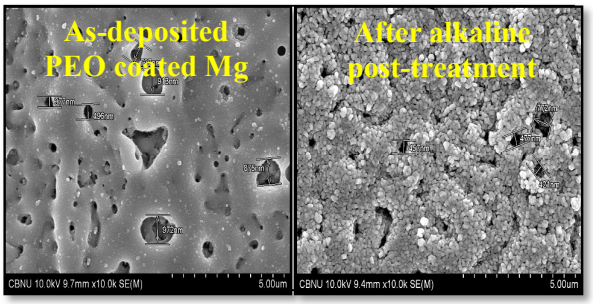

Post-treatment using 3 M NaOH at 60 °C for 1 h improves the performance of plasma electrolytic oxidation coated magnesium.